Electronic Supplementary Material (ESI) for Catalysis Science & Technology.

Supporting Information

Tuning Catalysis by Surface-Deposition of Elements on Oxidation Catalysts via Atomic Layer Deposition

Frederik Rüther,[a] Robert Baumgarten,[a] Fabian Ebert,[a] Esteban Gioria,[a]

Raoul Naumann d'Alnoncourt,[a†] Annette Trunschke,[b] and Frank Rosowski [c,a]

[a] BasCat - UniCat BASF JointLab, Technische Universität Berlin, D-10623 Berlin, Germany

[b] Department of Inorganic Chemistry, Fritz Haber Institute of the Max Planck Society, D-14195 Berlin, Germany

[c] BASF SE, Catalysis Research, D-67065 Ludwigshafen, Germany

[†] Corresponding Author; Email-address: r.naumann@bascat.tu-berlin.de

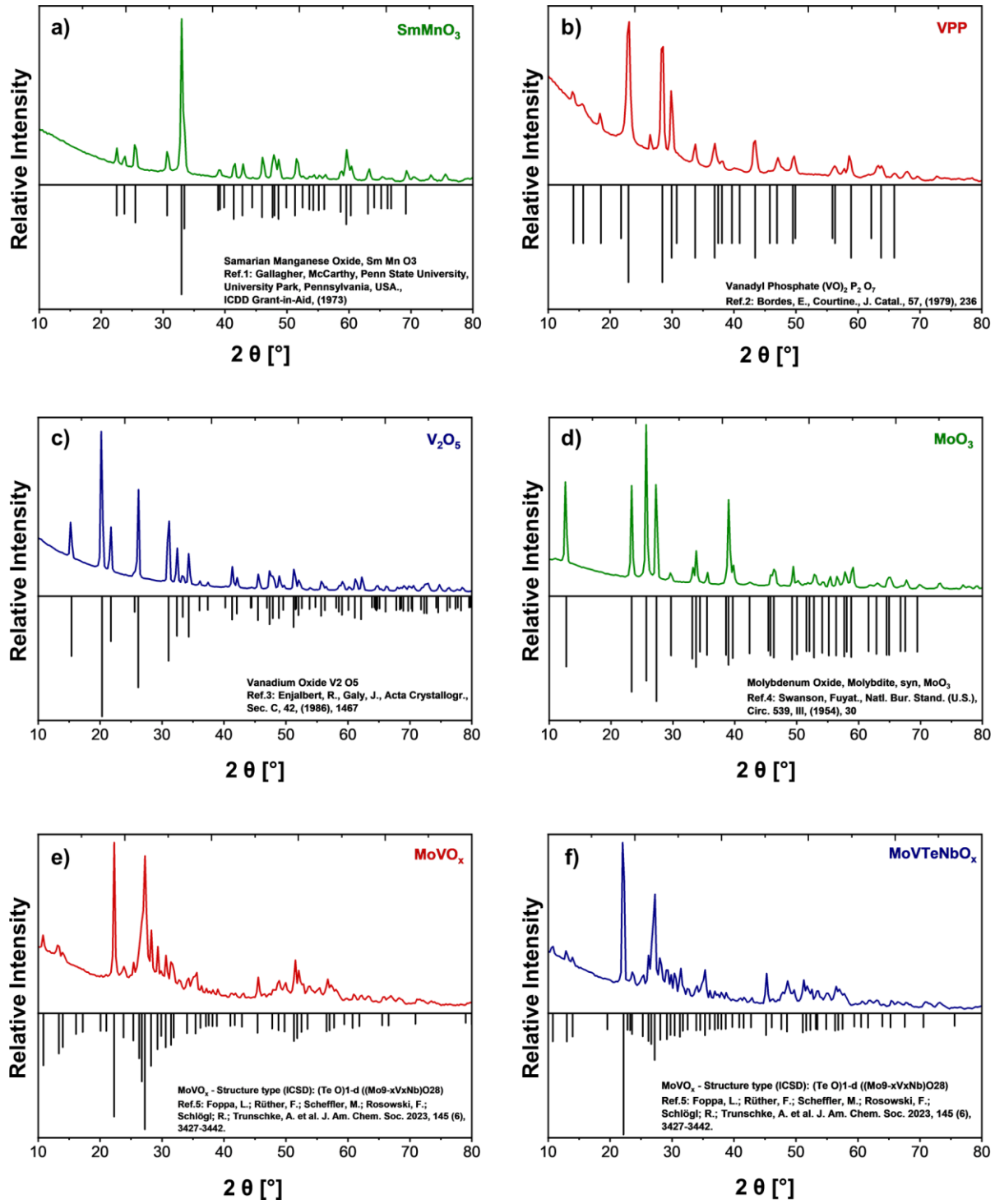

Figure SI1. XRPD patterns of the five base catalysts (a) $SmMnO_3$, (b) VPP, (c) V_2O_5, (d) MoO_3, (e) $MoVO_x$, and (f) $MoVTeNbO_x$ before catalysis (fresh) in the angular range $10° \leq 2\theta < 80°$, main reflections of reference crystal structures (a) $SmMnO_3$ [1], (b) VPP [2], (c) V_2O_5 [3], (d) MoO_3 [4], (e) $MoVO_x$ [5], and (f) $MoVTeNbO_x$ [5] shown below for phase identification.

Table SI1. Results of N_2-physisorption measurements of the six base catalysts $MoVTeNbO_x$, $MoVO_x$, MoO_3, V_2O_5, VPP, and $SmMnO_3$: Specific BET surface area and specific pore volume of fresh samples; Calculation according to the BJH pore size distribution based on the N_2-desorption.

Catalyst	**$MoVTeNbO_x$**	**$MoVO_x$**	**V_2O_5**	**VPP**	**MoO_3**	**$SmMnO_3$**
BET surface area [m^2/g]	7.7	36.2	6.6	25.6	3.1	7.5
Pore-V_{BJH} [cm^3/g]	0.016	0.172	0.025	0.181	0.015	0.028

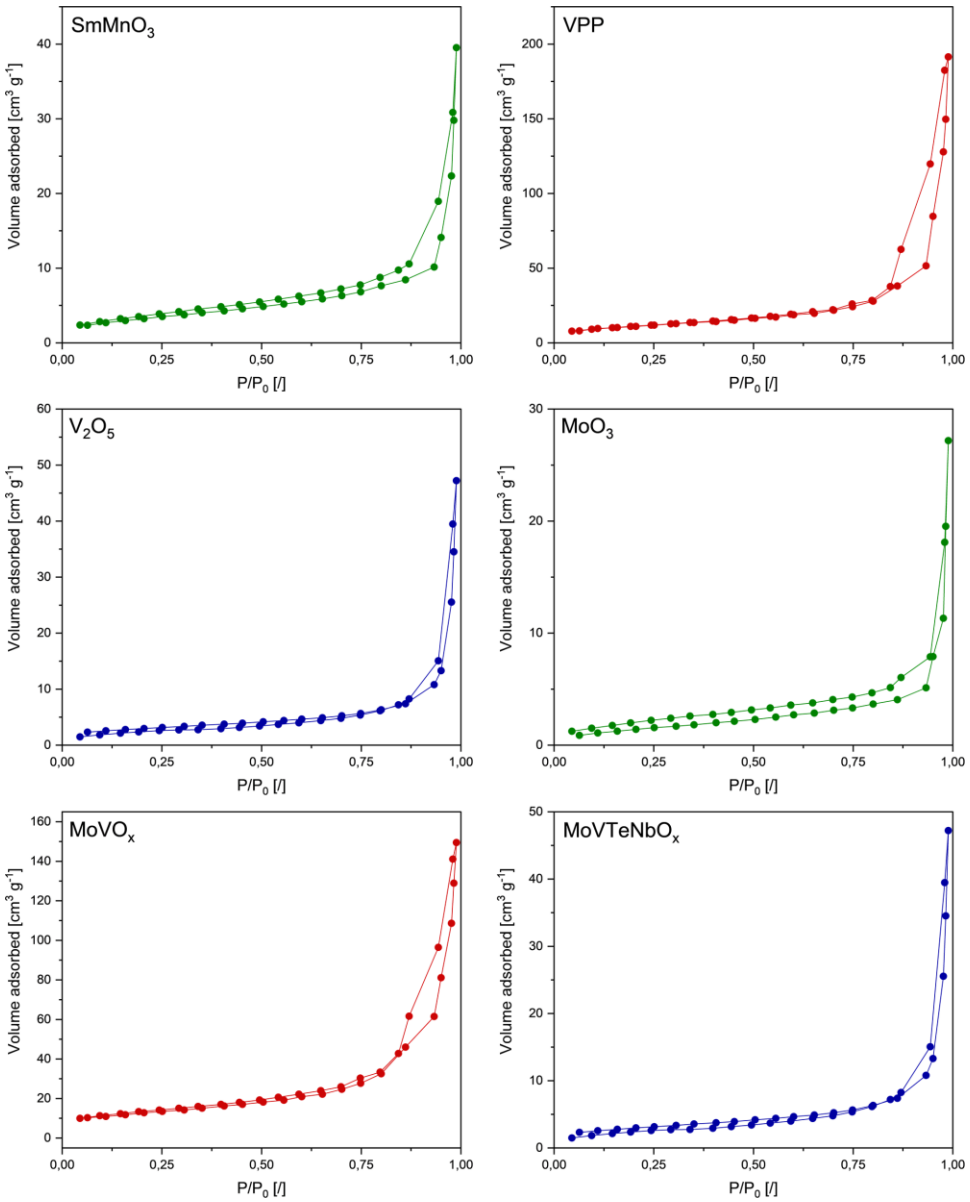

Figure SI2. N_2-physisorption measurement curves of adsorption and desorption: Comparison between the five base catalysts $MoVTeNbO_x$, $MoVO_x$, MoO_3, V_2O_5, VPP, and $SmMnO_3$ before catalysis (fresh).

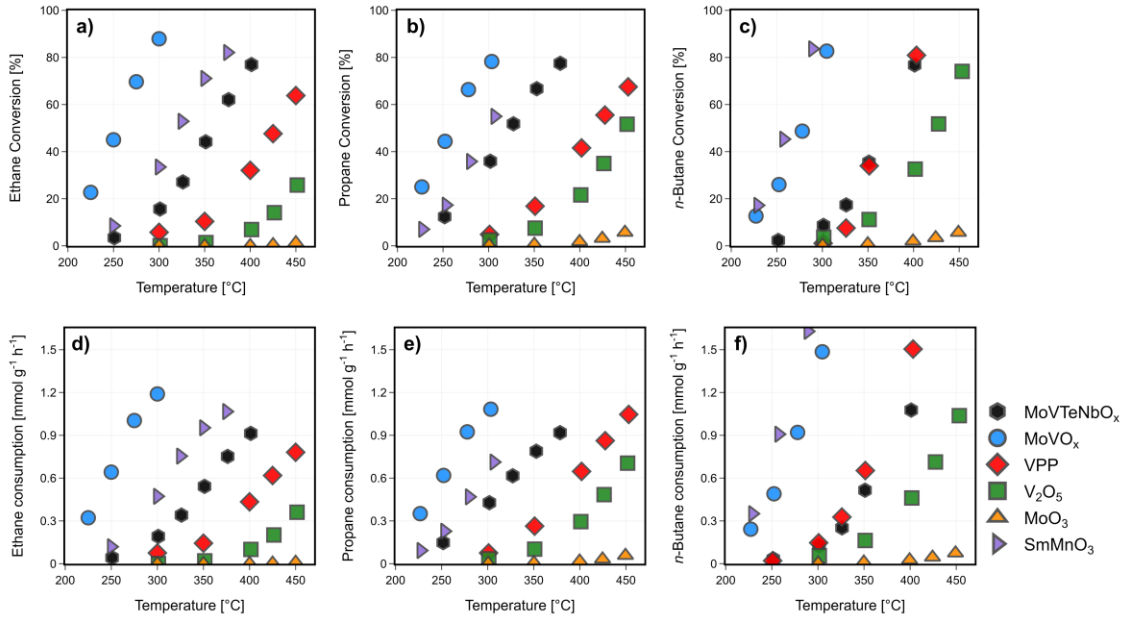

Figure SI3. Catalytic activity of $MoVTeNbO_x$, $MoVO_x$, MoO_3, V_2O_5, VPP, and $SmMnO_3$: Alkane conversion [%] and alkane consumption rates normalized to the catalyst mass [mmol g^{-1} h^{-1}] as a function of the reaction temperature in (a, d) ethane, (b, e) propane, and (c, f) *n*-butane oxidation; $C_2H_6/O_2/H_2O$=3/9/0 %vol, $C_3H_8/O_2/H_2O$=3/9/20 %vol, $C_4H_{10}/O_2/H_2O$=2/20/3 %vol, 1 atm, 1000 h^{-1} (C_2, C_3) / 2000 h^{-1} (C_4).

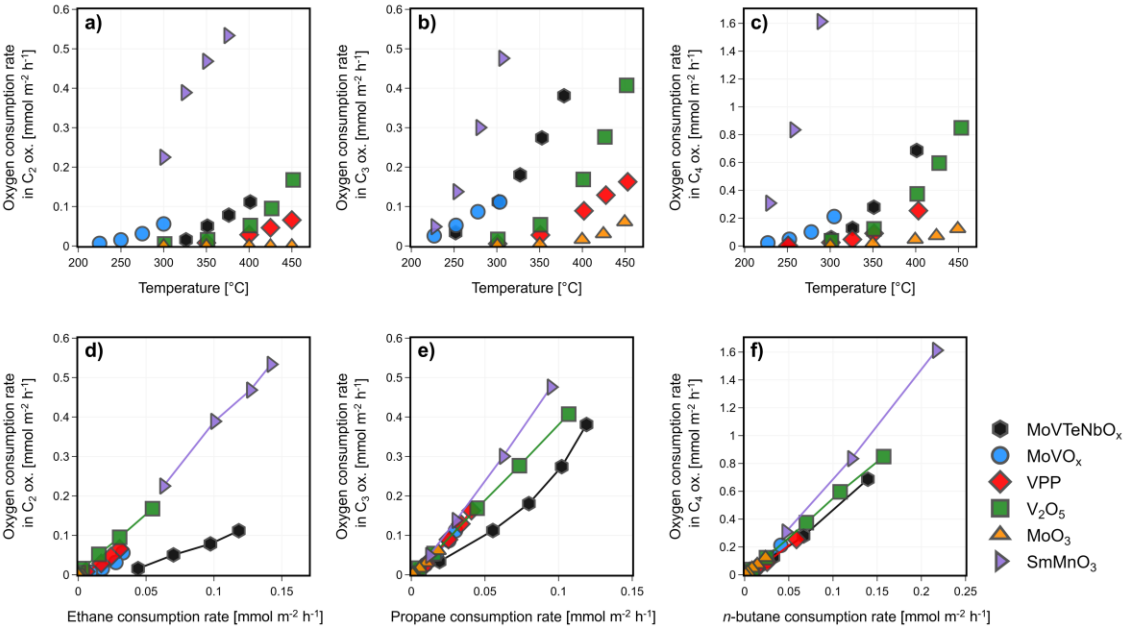

Figure SI4. Catalytic activity of $MoVTeNbO_x$, $MoVO_x$, MoO_3, V_2O_5, VPP, and $SmMnO_3$: Oxygen consumption rates normalized to the catalyst mass [mmol m^{-2} h^{-1}] as a function of the reaction temperature in (a) ethane, (b) propane, and (c) *n*-butane oxidation; oxygen consumption rate as a function of the consumption rate of the respective alkane (d) ethane, (e) propane, and (f) *n*-butane; $C_2H_6/O_2/H_2O$=3/9/0 %vol, $C_3H_8/O_2/H_2O$=3/9/20 %vol, $C_4H_{10}/O_2/H_2O$=2/20/3 %vol, 1 atm, 1000 h^{-1} (C_2, C_3) / 2000 h^{-1} (C_4).

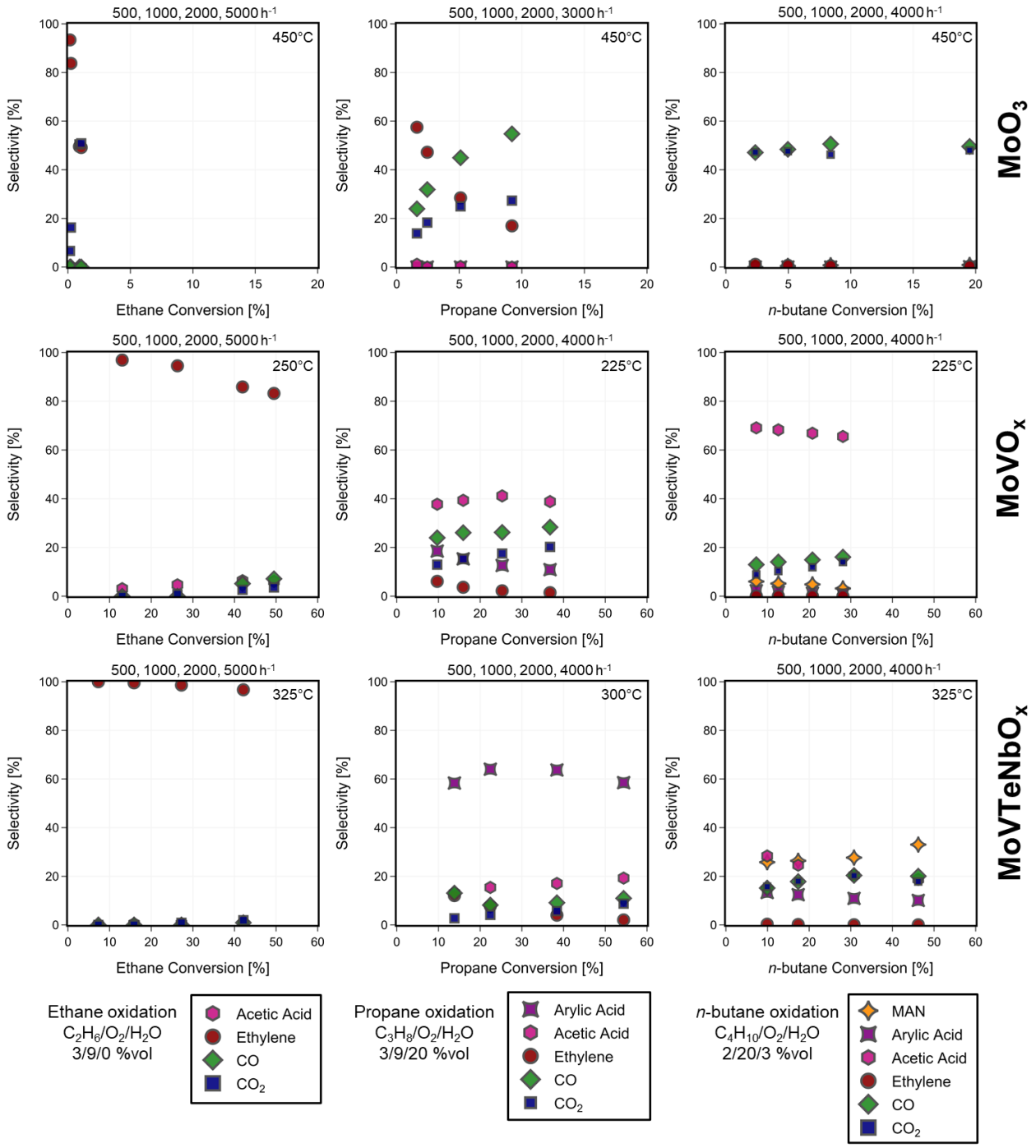

Figure SI5. GHSV variation study of MoO_3, $MoVO_x$, and $MoVTeNbO_x$: The temperature is fixed to a setpoint of X_{alkane} = 15% based on the previously performed temperature variation study; the temperature- and GHSV-setpoints are indicated within the diagrams; $C_2H_6/O2/H_2O$=3/9/0 %vol, $C_3H_8/O_2/H_2O$=3/9/20 %vol, $C_4H_{10}/O_2/H_2O$=2/20/3 %vol, 500 ≤ GHSV ≤ 5000, 1 atm.

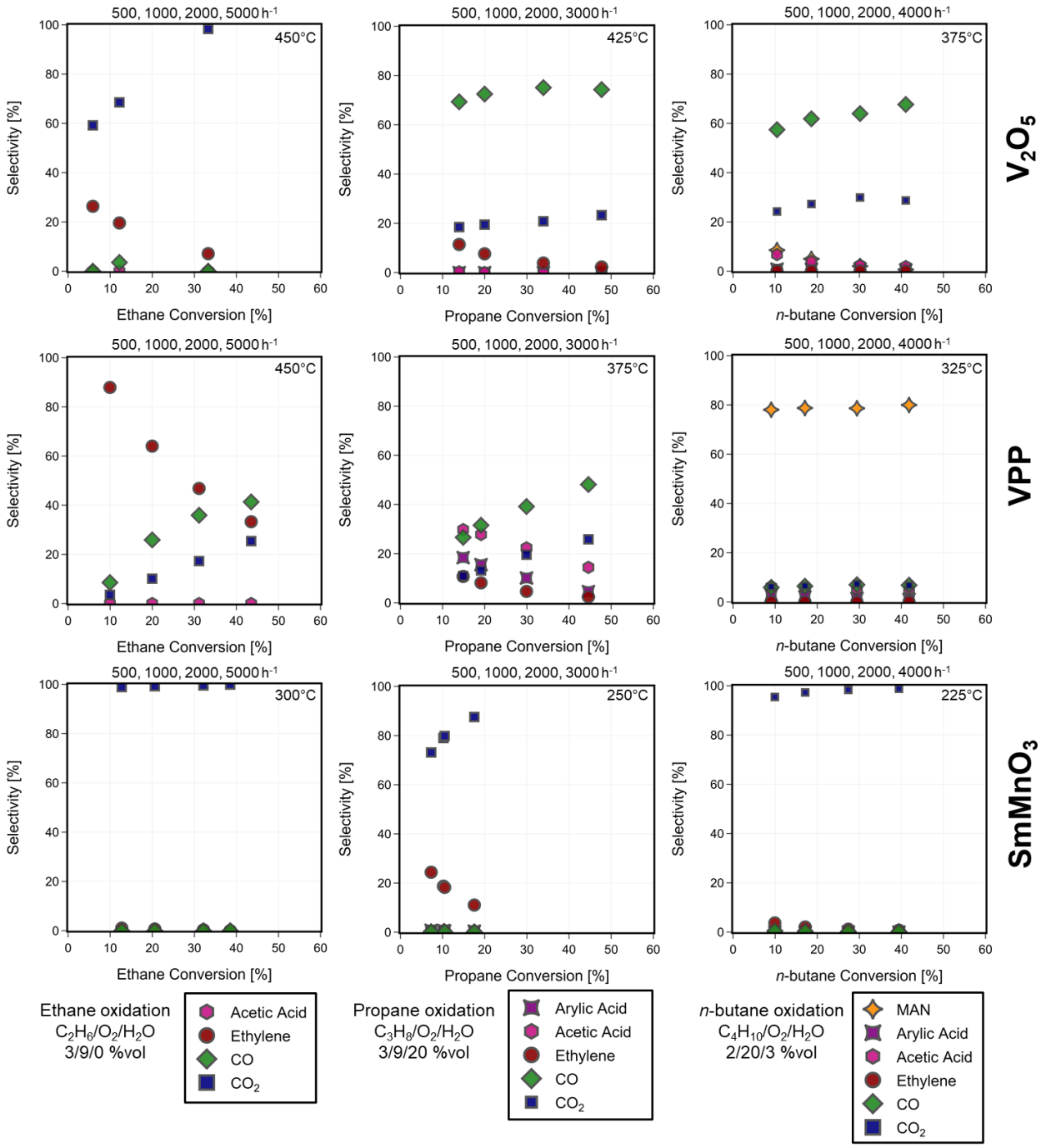

Figure SI6. GHSV variation study of V_2O_5, VPP, and $SmMnO_3$: The temperature is fixed to a setpoint of X_{alkane} = 15% based on the previously performed temperature variation study; the temperature- and GHSV-setpoints are indicated within the diagrams; $C_2H_6/O_2/H_2O$=3/9/0 %vol, $C_3H_8/O_2/H_2O$=3/9/20 %vol, $C_4H_{10}/O_2/H_2O$=2/20/3 %vol, 500 ≤ GHSV ≤ 5000, 1 atm.

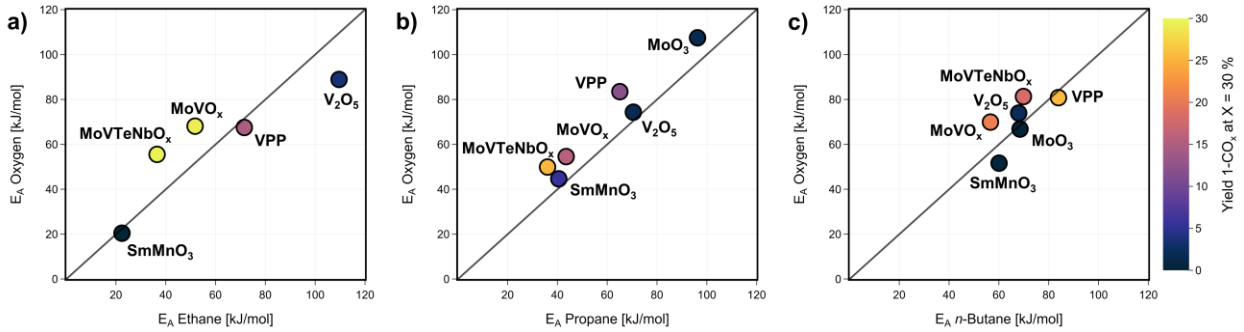

Figure SI7. Apparent activation energies of (a) ethane, (b) propane, (c) *n*-butane, and oxygen in respective reaction calculated based on the temperature variation study; Colour-coding indicates the yield towards partial oxidation products (1-CO_x); Due to the very low conversion the activation energies of MoO_3 in ethane oxidation are not defined; $C_2H_6/O_2/H_2O$=3/9/0 %vol, $C_3H_8/O_2/H_2O$=3/9/20 %vol, $C_4H_{10}/O_2/H_2O$=2/20/3 %vol, 1 atm, 1000 h^{-1} (C_2, C_3) / 2000 h^{-1} (C_4).

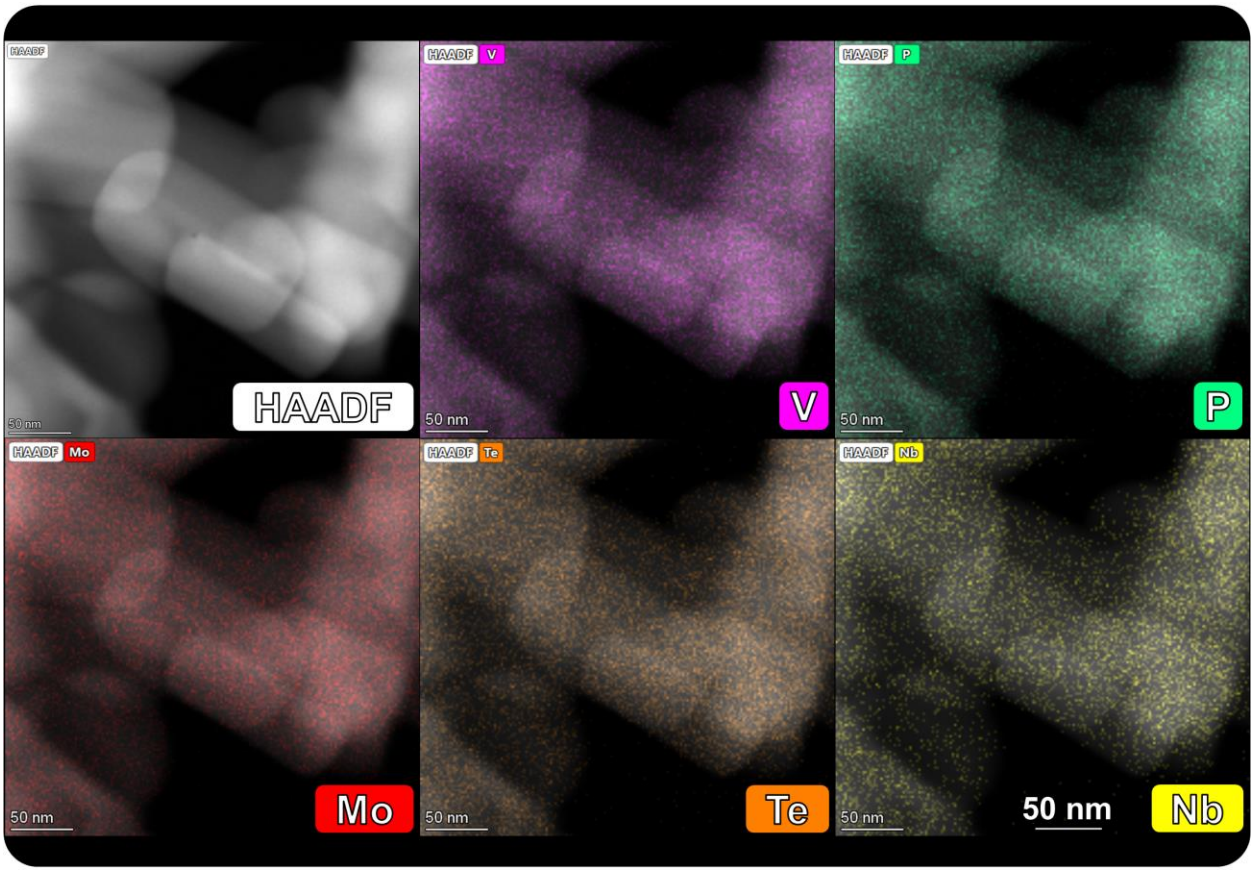

Figure SI8. STEM-HAADF images (50 nm) of PO_x surface modified $MoVTeNbO_x$ before catalysis (fresh sample): EDX-mappings show element dispersion of both bulk elements (Mo, V, Te, Nb) and the additionally deposited phosphorus (PO_x).

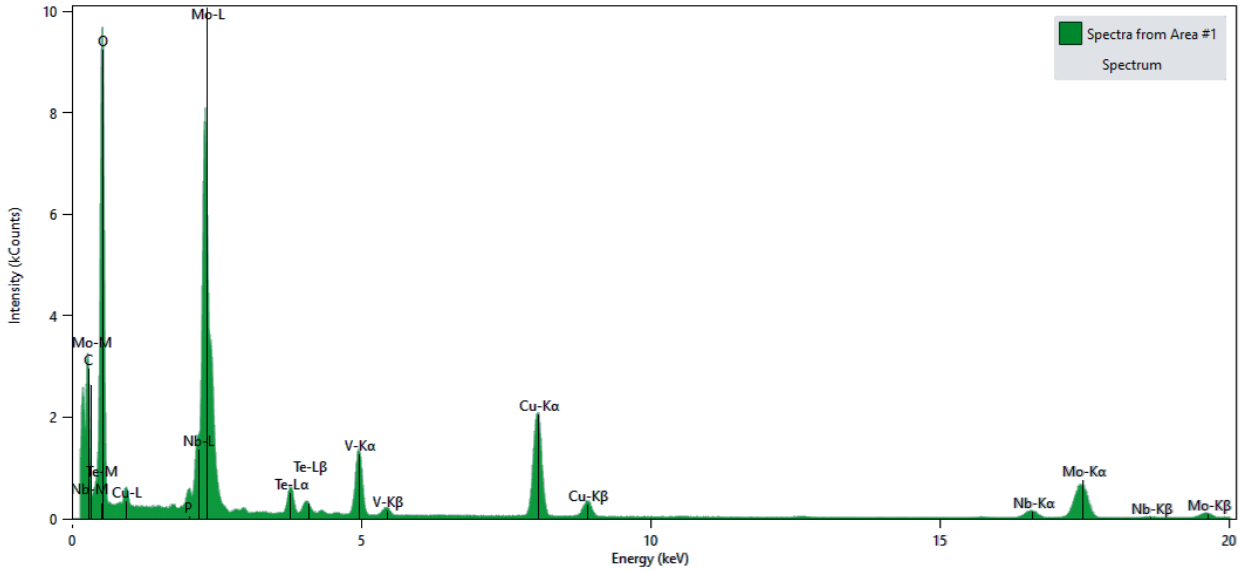

Figure SI9. STEM-EDX mapping spectra of PO_x surface modified $MoVTeNbO_x$ after catalysis (spent sample).

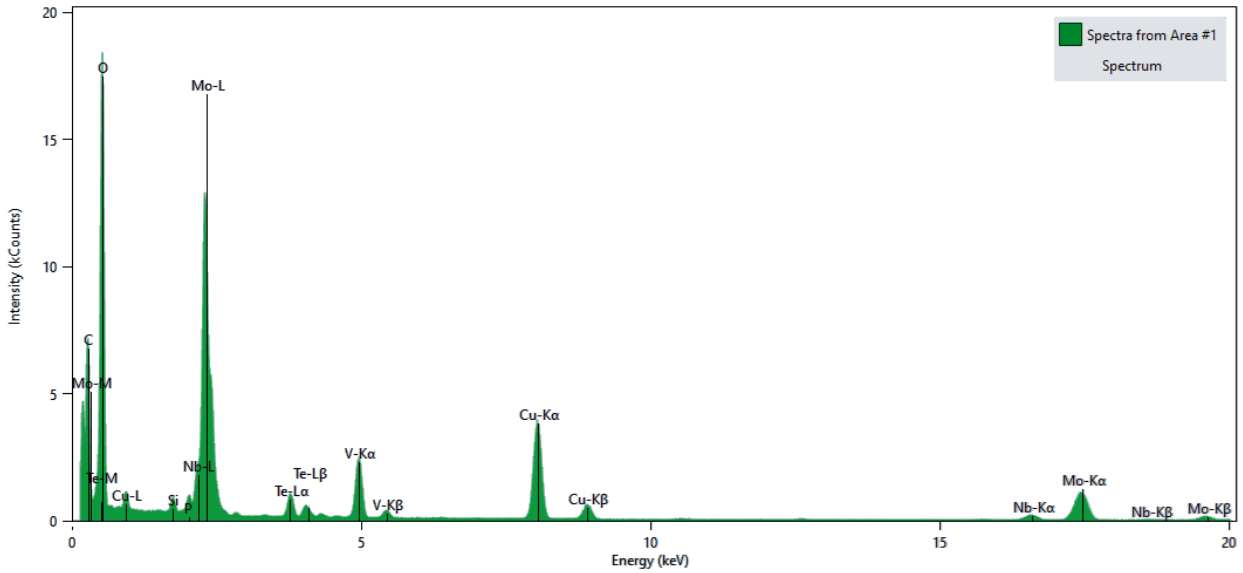

Figure SI10. STEM-EDX mapping spectra of PO_x surface modified $MoVTeNbO_x$ before catalysis (fresh sample).

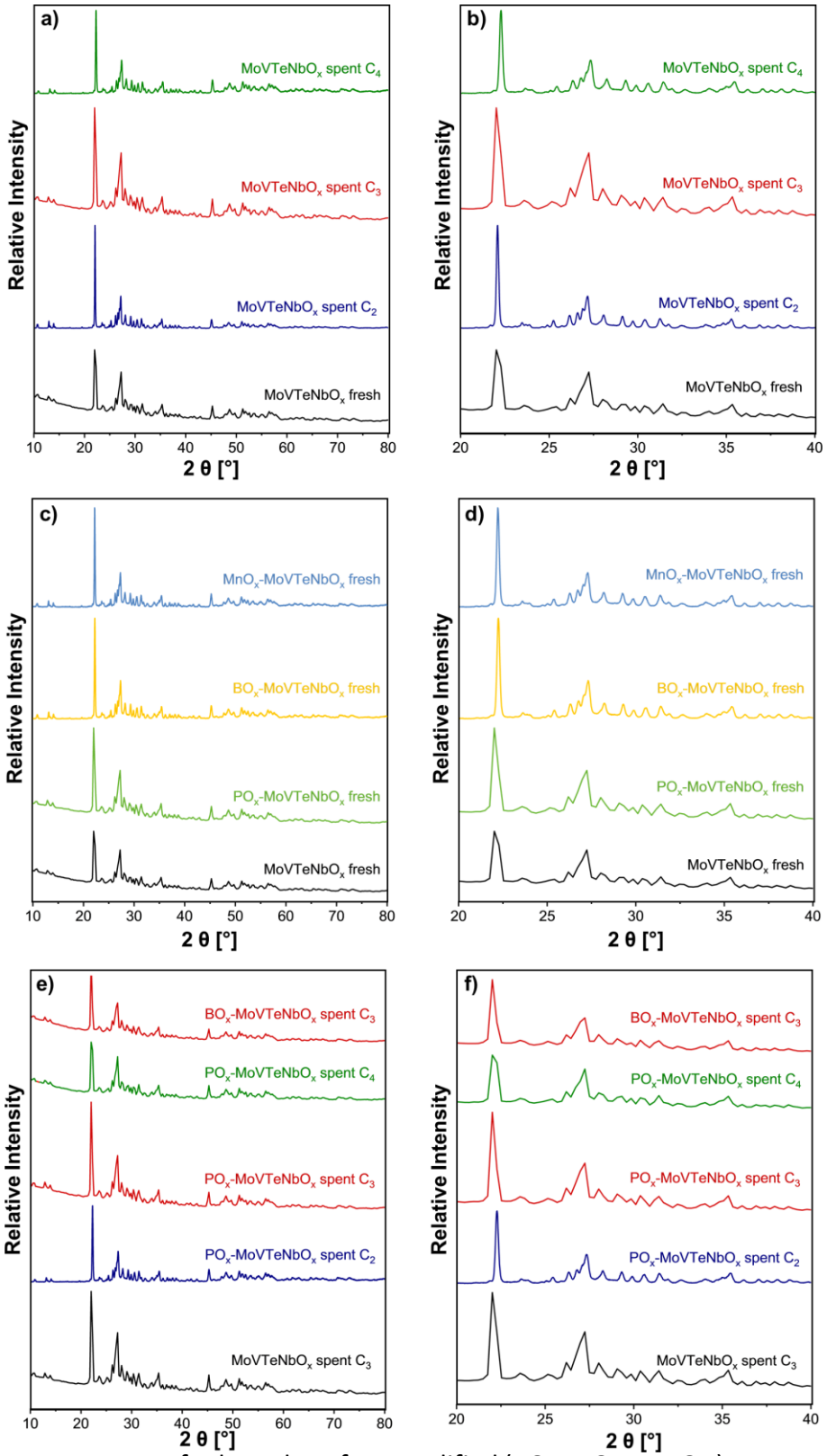

Figure SI11. XRPD patterns of selected, surface modified (BO_x-, PO_x-, MnO_x-) $MoVTeNbO_x$ samples before (fresh) and after (spent) catalysis (C_2, C_3, C_4) in the angular range of (a, c, d) $10° \leq 2\theta < 80°$ and (b, d, f) $20° \leq 2\theta < 40°$: Comparison between patterns of (a, b) base catalyst samples after different reactions, (c, d) surface modified (fresh) samples after ALD, (e, f) surface modified samples after catalysis.

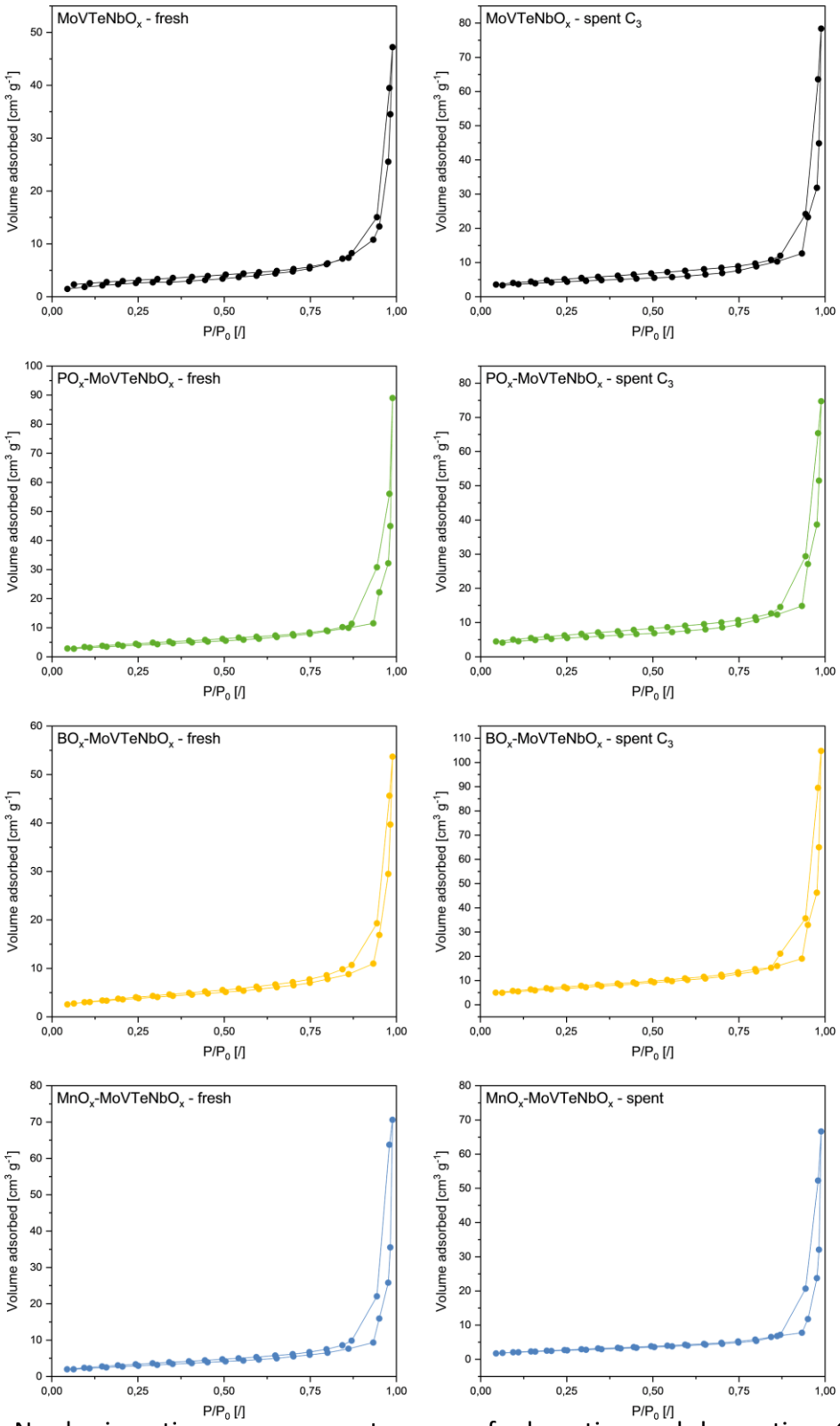

Figure SI12. N_2-physisorption measurement curves of adsorption and desorption: Comparison between the base catalyst and the surface modified (BO_x-, PO_x-, MnO_x-) $MoVTeNbO_x$ samples before (fresh) and after (spent) catalysis.

Table SI2. Results of N_2-physisorption measurements of surface modified (BO_x-, PO_x-, MnO_x-) $MoVTeNbO_x$: Specific BET-surface area before and after catalytic studies in the selective oxidation of propane; Pore volume calculated according to the BJH pore size distribution based on the N_2-desorption.

	$MoVTeNbO_x$	BO_x-$MoVTeNbO_x$	PO_x-$MoVTeNbO_x$	MnO_x-$MoVTeNbO_x$
BET Surface area, fresh [m^2/g]	7.7	7.0	6.2	7.9
BET Surface area, spent C_3 [m^2/g]	7.7	7.9	7.1	7.1
Pore-V_{BJH} fresh [cm^3/g]	0.016	0.037	0.038	0.077
Pore-V_{BJH} spent [cm^3/g]	0.050	0.046	0.038	0.065

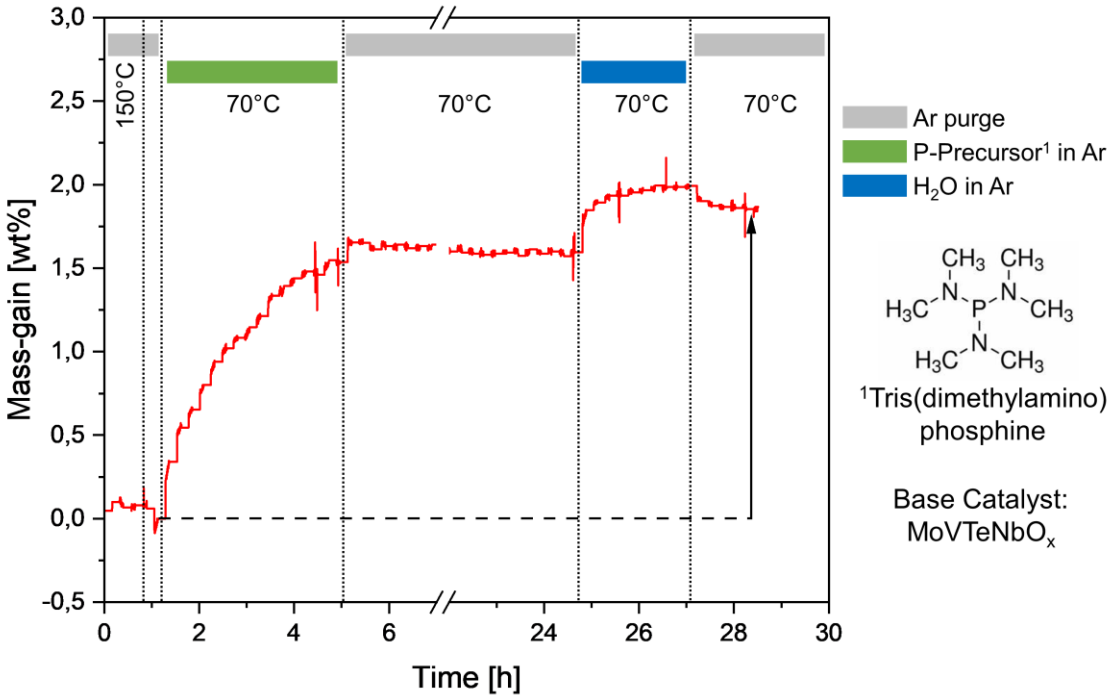

Figure SI13. Gravimetric monitoring (*in situ*) of the PO_x-ALD-process; exemplary the deposition of PO_x on $MoVTeNbO_x$ as base catalyst is presented. One ALD-cycle can be divided into two sequential solid-gas reactions or half-cycles, in which (1) the respective element precursor is dosed until saturation leading to a mass gain by surface deposition, then (2) the ligand is removed using water in Ar. In case of PO_x-ALD all steps are proceeded at 70°C.

Table SI3. Results of XPS measurements of surface modified (BO_x-, PO_x-, MnO_x-)$MoVTeNbO_x$: Near-surface composition in atomic% before and after catalytic studies in propane oxidation; Ratio R between the different oxidation states of V found at the near-surface.

Catalyst	Mo [%at]	V $2p_{3/2}$ [%at]	Te [%at]	Nb $3d_{5/2}$ [%at]	O 1s [%at]	B/P/Mn [%at]	R=V^{4+}/ (V^{4+}+V^{5+})
$MoVTeNbO_x$-fresh	19.90	1.71	2.66	3.21	72.52	/	0.55
$MoVTeNbO_x$-spent	19.13	1.80	2.81	3.22	73.04	/	0.66
BO_x-$MoVTeNbO_x$-fresh	18.94	1.75	2.64	3.19	72.30	1,19	0.68
BO_x-$MoVTeNbO_x$-spent	19.79	1.73	2.63	3.23	72.62	n.d.	0.56
PO_x-$MoVTeNbO_x$-fresh	16.80	1.50	2.08	3.03	73.16	3.43	0.58
PO_x-$MoVTeNbO_x$-spent	18.31	1.71	2.54	3.01	72.47	1.96	0.50
MnO_x-$MoVTeNbO_x$-fresh	15.07	1.45	2.17	2.48	72.48	6.34	0.72
MnO_x-$MoVTeNbO_x$-spent	17.81	1.78	2.20	3.43	72.05	2.72	0.71

Table SI4. Results of ICP-OES and XPS measurements of surface modified (BO_x-, PO_x-) $MoVTeNbO_x$: Element composition as atomic ratios and mass fractions before and after catalytic studies in the selective oxidation of propane.

Catalyst	Mo [%at]	V [%at]	Te [%at]	Nb [%at]	O [%at]	B [%at]	P [%at]
BO_x-$MoVTeNbO_x$-fresh-ICP-OES	19.27	2.93	2.40	2.36	70.10	2.94	0.00
BO_x-$MoVTeNbO_x$-spent-ICP-OES	18.69	2.92	2.26	2.31	72.76	1.05	0.00
PO_x-$MoVTeNbO_x$-fresh-ICP-OES	19.40	2.89	2.39	2.34	72.05	0.00	0.94
PO_x-$MoVTeNbO_x$-spent-ICP-OES	18.58	2.83	2.27	2.26	73.45	0.00	0.60
	Mo [%wt]	**V [%wt]**	**Te [%wt]**	**Nb [%wt]**	**O [%wt]**	**B [%wt]**	**P [%wt]**
BO_x-$MoVTeNbO_x$-fresh-ICP-OES	50.28	4.06	8.33	5.96	31.37	0.87	0.00
BO_x-$MoVTeNbO_x$-spent-ICP-OES	49.52	4.12	7.96	5.94	32.47	0.32	0.00
PO_x-$MoVTeNbO_x$-fresh-ICP-OES	50.14	3.97	8.22	5.85	31.84	0.00	0.79
PO_x-$MoVTeNbO_x$-spent-ICP-OES	49.23	3.99	8.02	5.81	32.97	0.00	0.52

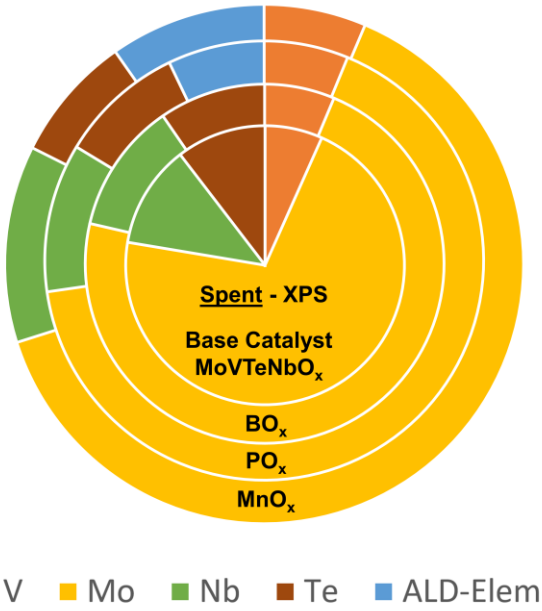

Figure SI14. Impact on near-surface composition (at%) by surface modification (BO_x-, PO_x-, MnO_x-) of the $MoVTeNbO_x$ catalyst after propane oxidation (spent) determined by XPS measurements; the oxygen content is excluded for the visualization.

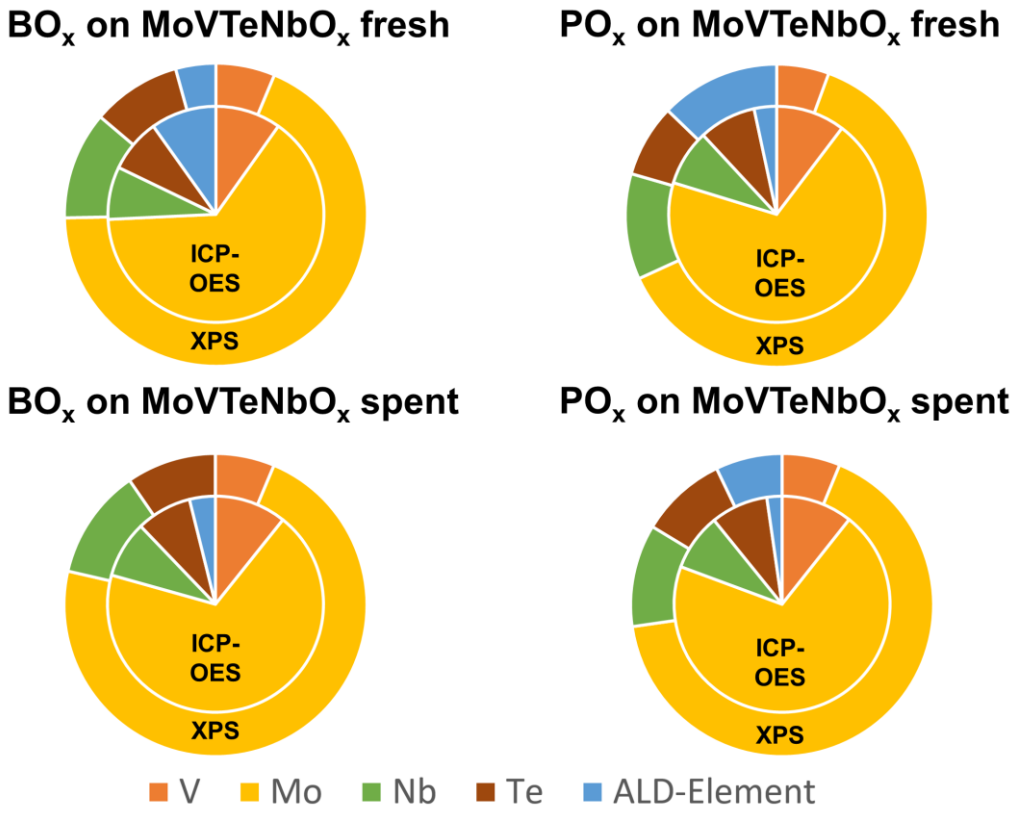

Figure SI15. Comparison between near-surface (XPS) and bulk composition (ICP-OES) (at%) of surface modified (BO_x-, PO_x-) $MoVTeNbO_x$ catalyst before (fresh) and after propane oxidation (spent); the oxygen content is excluded for the visualization.

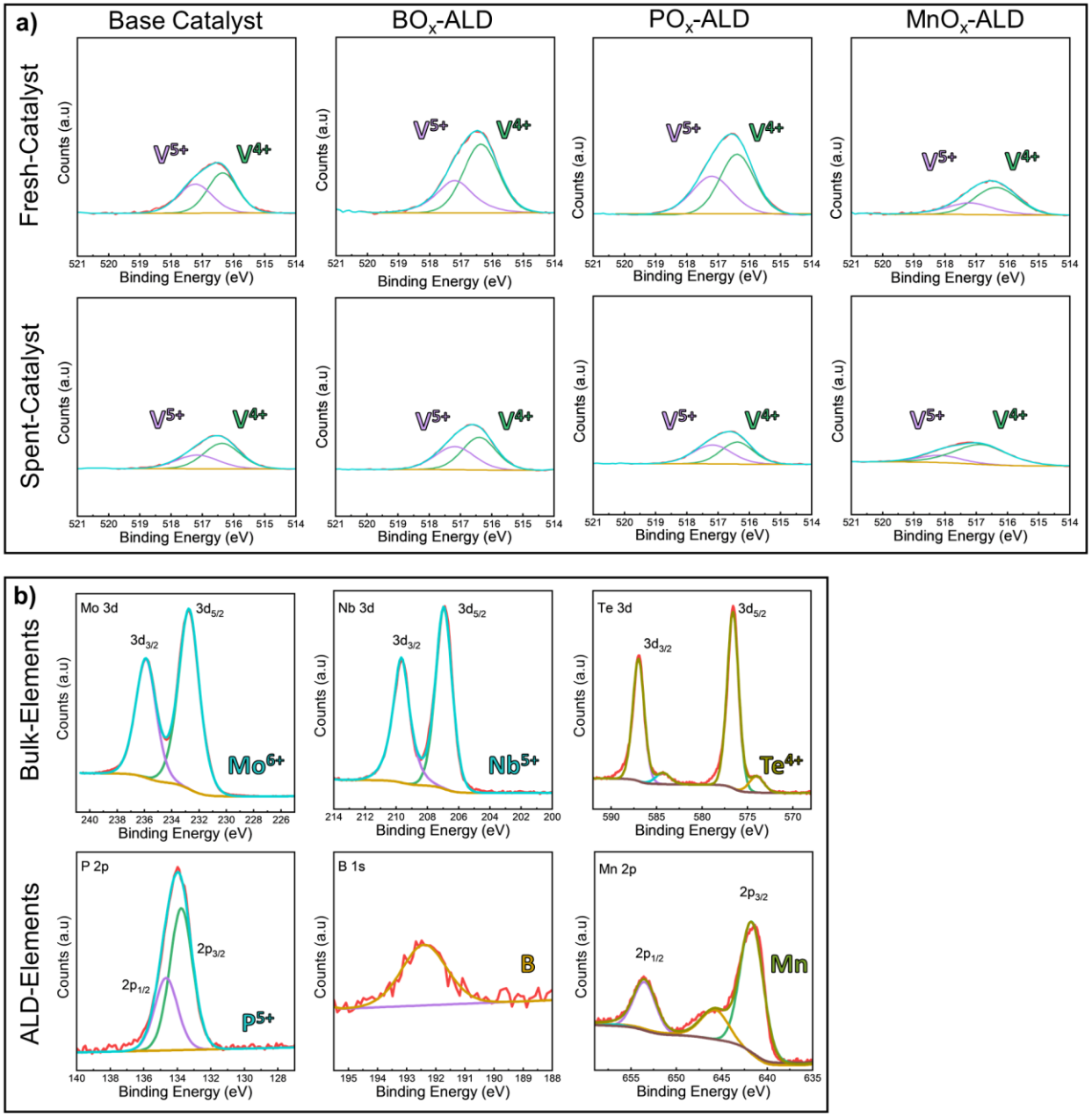

Figure SI16. XPS spectra of surface modified (BO_x-, PO_x-, MnO_x-) $MoVTeNbO_x$: The two peaks located at 517.21 eV and 516.38 eV, correspond to V^{5+} and V^{4+}, respectively; The spectra for Nb 3d region depict two peaks located at 206.9 eV and 209.7 eV, correspond to $3d_{5/2}$ and $3d_{3/2}$ core level of Nb^{5+}, in all samples. The spectra for Mo 3d region depict two peaks located at 232.7 eV and 235.9 eV, correspond to $3d_{5/2}$ and $3d_{3/2}$ core level of Mo^{6+}, respectively. For all samples, the spectra for Te 3d region depicts two peaks located at 576.6 eV and 586.9 eV, correspond to $3d_{5/2}$ and $3d_{3/2}$ core level of Te^{4+}, together with the characteristics sub-oxide peaks at 573.9 eV and 584.3 eV. The two peaks located at 133.7 eV and 134.6 eV, correspond to $2p_{3/2}$ and $2p_{1/2}$ core level of P^{5+}. (a) $2p_{3/2}$ region are shown before and after catalytic studies in propane oxidation, indicating the presence of V^{4+} and V^{5+} species. (b) Exemplary spectra for Mo^{6+}, Te^{4+}, Nb^{5+}, B , P^{5+} and Mn are shown due a high overall similarity.

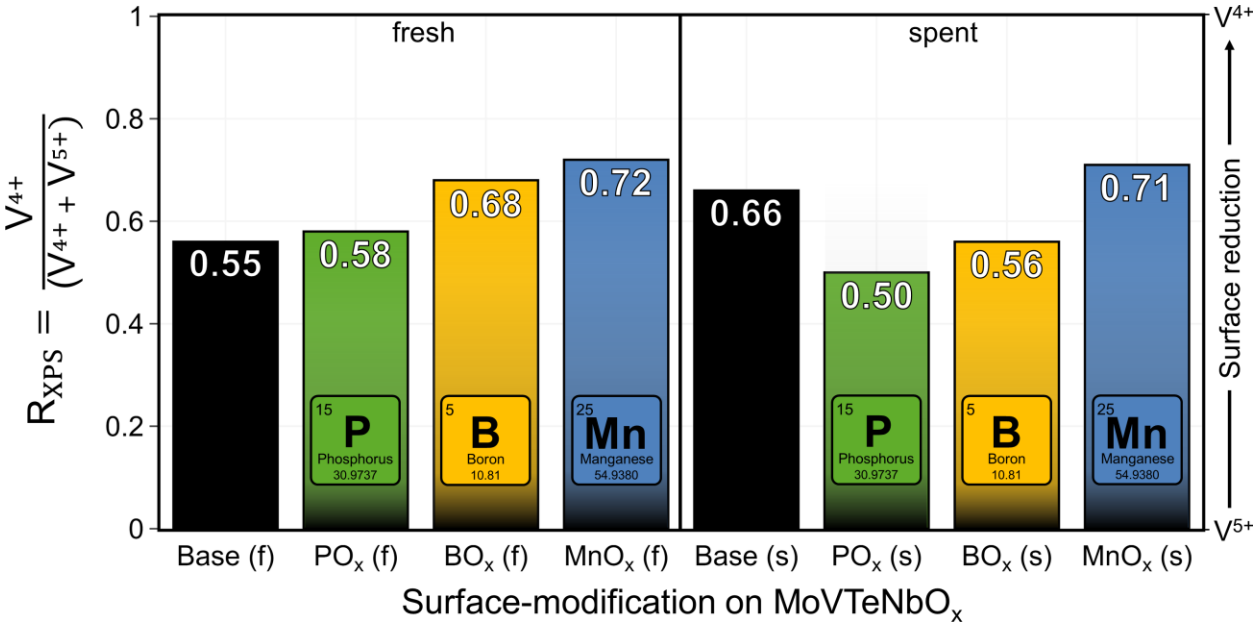

Figure SI17. Effect of surface deposition of BO_x, PO_x, MnO_x on the electronic environment of near-surface V-sites on $MoVTeNbO_x$ before (fresh) and after catalysis in propane oxidation (spent); Ratio between reduced V^{4+} species and the sum of V^{4+} and V^{5+} calculated from the XPS spectra in the of V $2p_{3/2}$ region.

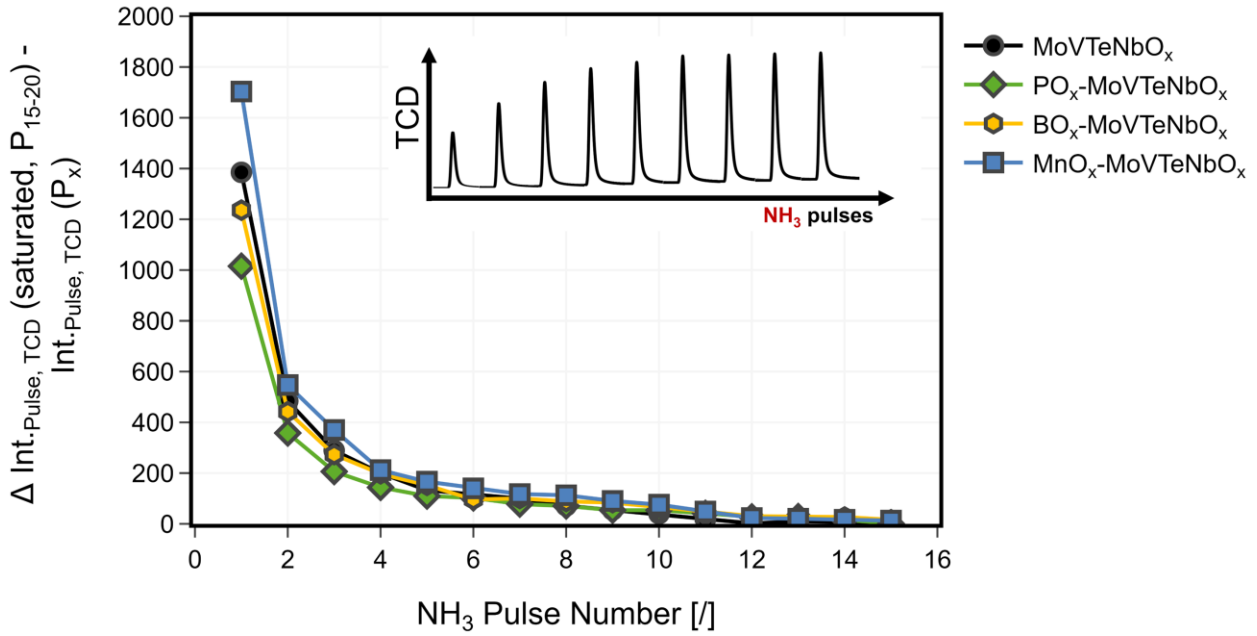

Figure SI18. NH_3-pulsing study of surface modified (BO_x-, PO_x-, MnO_x-) $MoVTeNbO_x$ samples at 90°C: Difference between the pulse integral (TCD) and the averaged pulse integral at saturation (Pulse 16 - Pulse 20) as a function of the number of the NH_3-pulses.

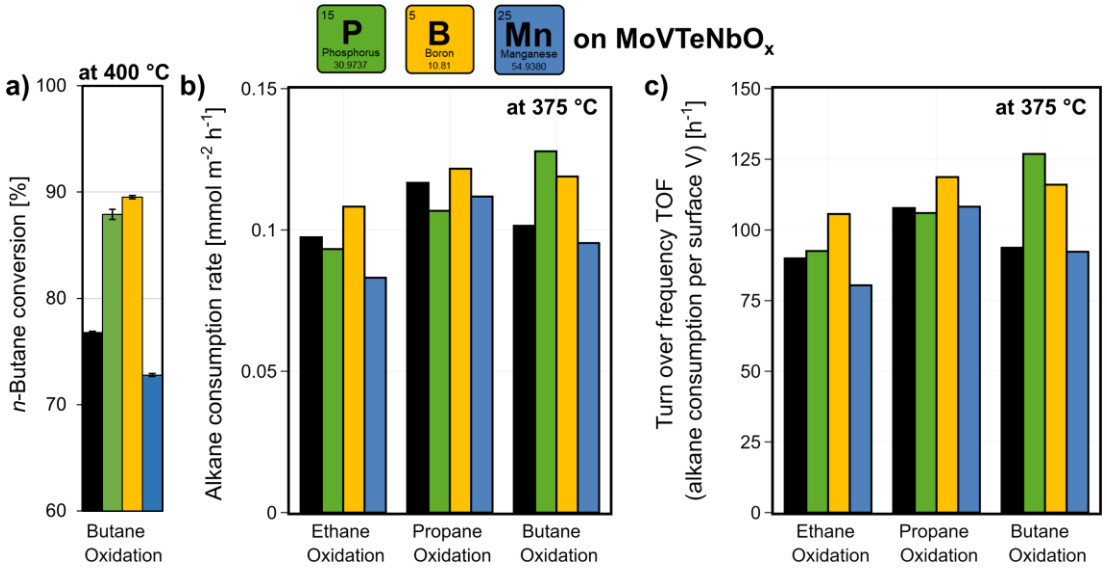

Figure SI19. Change in catalytic activity by surface modification with BO_x, PO_x, MnO_x on $MoVTeNbO_x$: (a) *n*-Butane conversion shown exemplary at 400°C with error-bars based on the four iteration measurements at one setpoint, (b) Alkane consumption rate at a fixed temperature setpoint of 375°C in ethane, propane, and *n*-butane oxidation; (c) Turn over frequency (TOF) of the respective alkane per V at the near-surface, determined by XPS-measurements of the spent samples at 375°C. The V-density at the near-surface was calculated based on the sum of metal atoms within the a-b plane of the unit cell of phase pure $MoVTeNbO_x$ with M1-structure type [6], the lattice parameter or dimensions determined [7], and the amount of V determined by XPS. $C_2H_6/O_2/H_2O$=3/9/0 %vol, $C_3H_8/O_2/H_2O$=3/9/20 %vol, $C_4H_{10}/O_2/H_2O$=2/20/3 %vol, 1 atm, 1000 h^{-1} (C_2, C_3) / 2000 h^{-1} (C_4).

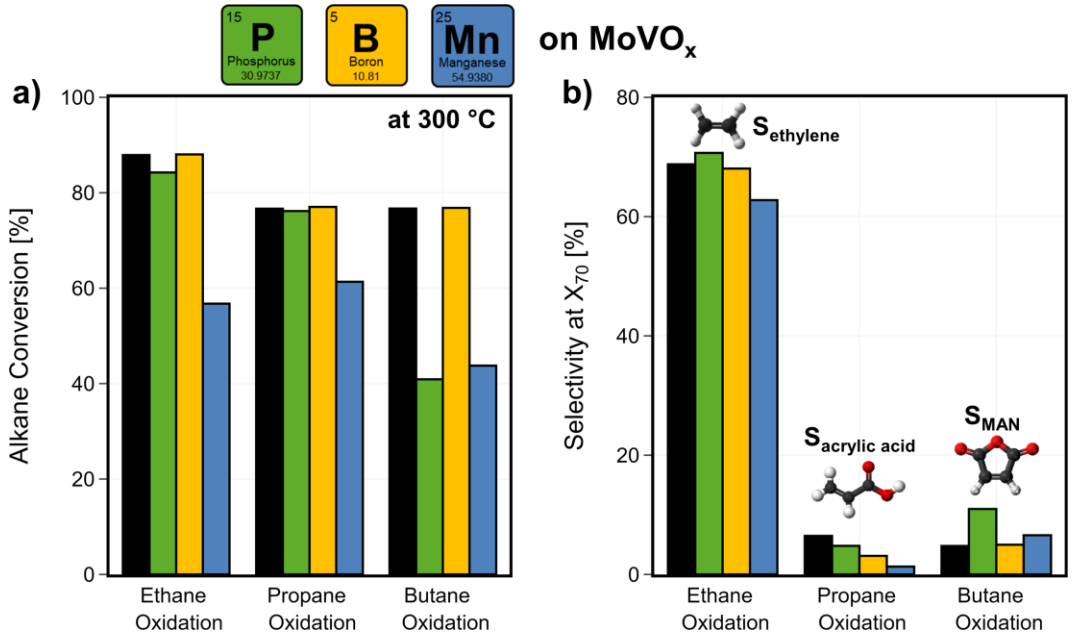

Figure SI20. Catalytic impact of surface modification with BO_x, PO_x, MnO_x on $MoVO_x$: (a) Change in alkane conversion at a fixed temperature setpoint of 300°C and (b) target-product selectivity (C_2: ethylene, C_3: acrylic acid, C_4: MAN) at a fixed conversion level of X_{alkane} = 70% (interpolated) in ethane, propane, and *n*-butane oxidation. $C_2H_6/O_2/H_2O$=3/9/0 %vol, $C_3H_8/O_2/H_2O$=3/9/20 %vol, $C_4H_{10}/O_2/H_2O$=2/20/3 %vol, 1 atm, 1000 h^{-1} (C_2, C_3) / 2000 h^{-1} (C_4).

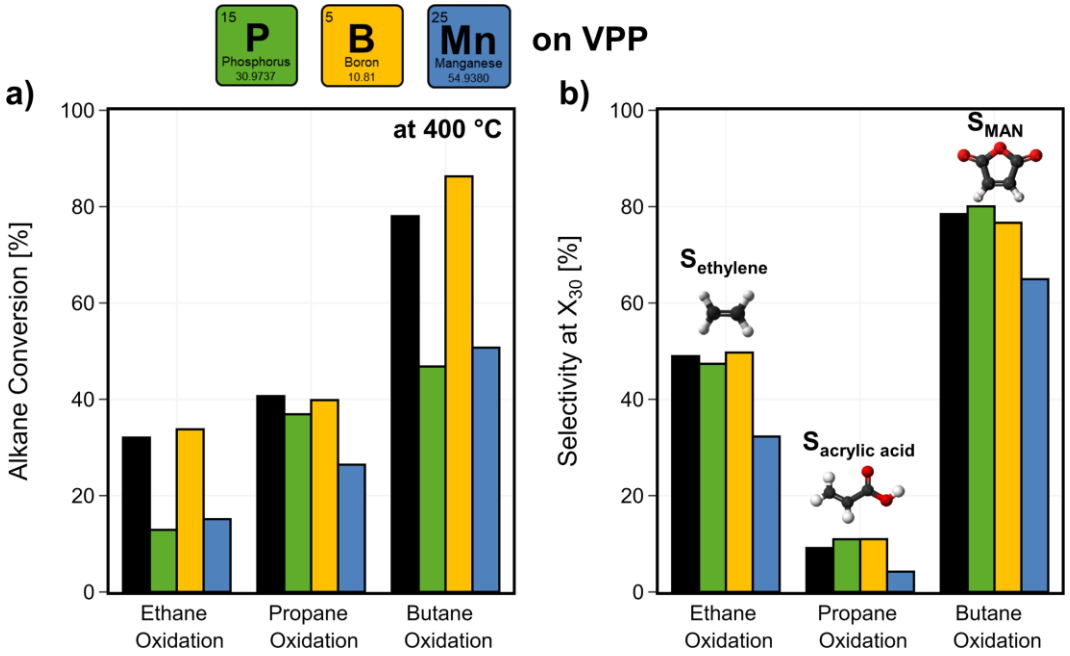

Figure SI21. Catalytic impact of surface modification with BO_x, PO_x, MnO_x on VPP: (a) Change in alkane conversion at a fixed temperature setpoint of 400°C and (b) target-product selectivity (C_2: ethylene, C_3: acrylic acid, C_4: MAN) at a fixed conversion level of X_{alkane} = 30% (interpolated) in ethane, propane, and *n*-butane oxidation. $C_2H_6/O_2/H_2O$=3/9/0 %vol, $C_3H_8/O_2/H_2O$=3/9/20 %vol, $C_4H_{10}/O_2/H_2O$=2/20/3 %vol, 1 atm, 1000 h^{-1} (C_2, C_3) / 2000 h^{-1} (C_4).

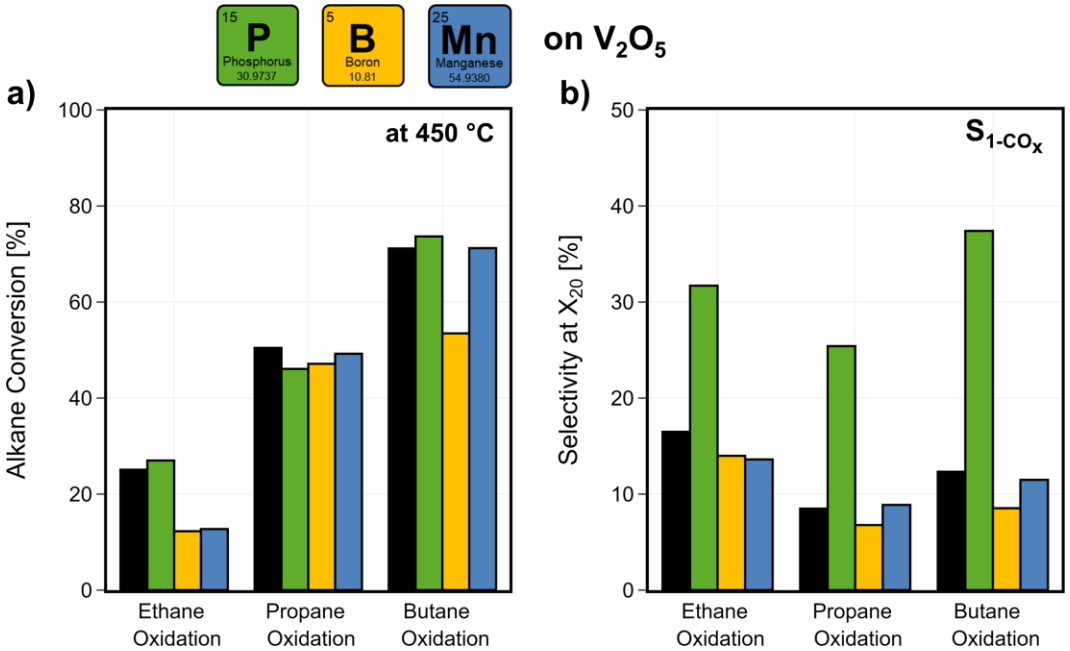

Figure SI22. Catalytic impact of surface modification with BO_x, PO_x, MnO_x on V_2O_5: (a) Change in alkane conversion at a fixed temperature setpoint of 450°C and (b) selectivity towards partial oxidation products (1-CO_x) at a fixed conversion level of X_{alkane} = 20% (interpolated) in ethane, propane, and *n*-butane oxidation. $C_2H_6/O_2/H_2O$=3/9/0 %vol, $C_3H_8/O_2/H_2O$=3/9/20 %vol, $C_4H_{10}/O_2/H_2O$=2/20/3 %vol, 1 atm, 1000 h^{-1} (C_2, C_3) / 2000 h^{-1} (C_4).

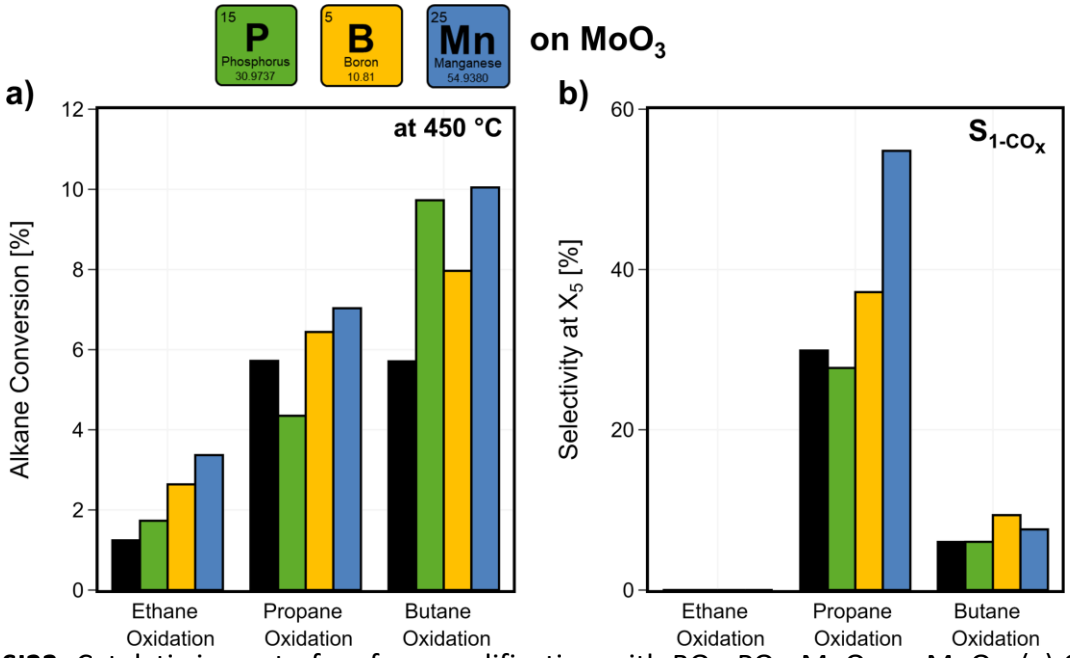

Figure SI23. Catalytic impact of surface modification with BO_x, PO_x, MnO_x on MoO_3: (a) Change in alkane conversion at a fixed temperature setpoint of 450°C and (b) selectivity towards partial oxidation products (1-CO_x) at a fixed conversion level of X_{alkane} = 5% (interpolated) in ethane, propane, and *n*-butane oxidation; Selectivities in C_2 oxidation not shown due to low conversion. $C_2H_6/O_2/H_2O$=3/9/0 %vol, $C_3H_8/O_2/H_2O$=3/9/20 %vol, $C_4H_{10}/O_2/H_2O$=2/20/3 %vol, 1 atm, 1000 h^{-1} (C_2, C_3) / 2000 h^{-1} (C_4).

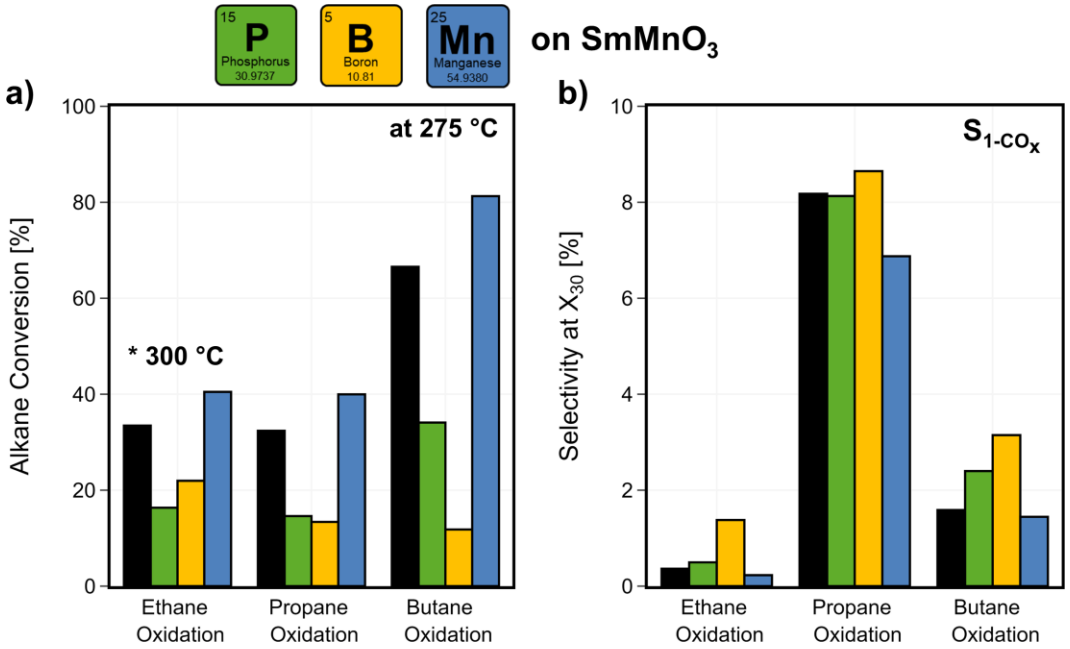

Figure SI24. Catalytic impact of surface modification with BO_x, PO_x, MnO_x on $SmMnO_3$: (a) Change in alkane conversion at fixed temperature setpoints of 275°C and 300°C and (b) selectivity towards partial oxidation products (1-CO_x) at a fixed conversion level of X_{alkane} = 30% (interpolated) in ethane, propane, and *n*-butane oxidation. $C_2H_6/O_2/H_2O$=3/9/0 %vol, $C_3H_8/O_2/H_2O$=3/9/20 %vol, $C_4H_{10}/O_2/H_2O$=2/20/3 %vol, 1 atm, 1000 h^{-1} (C_2, C_3) / 2000 h^{-1} (C_4).

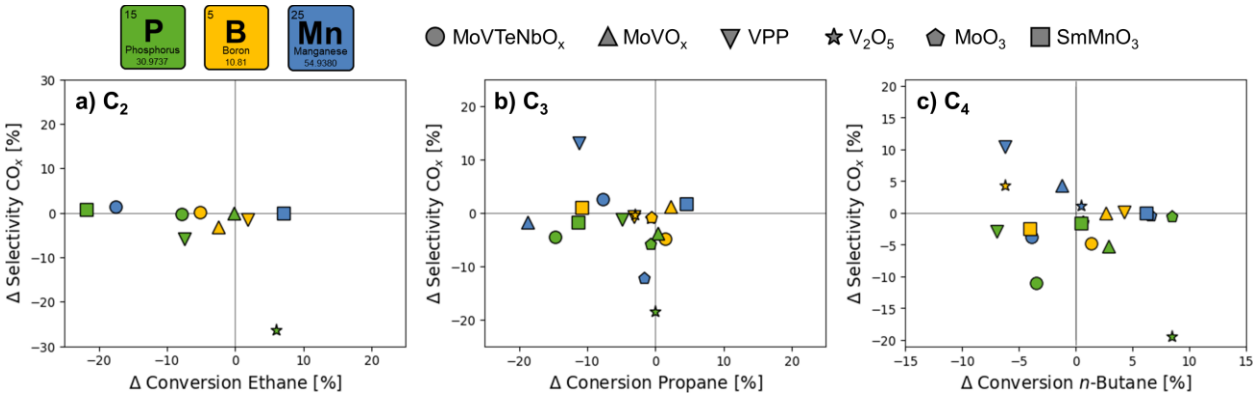

Figure SI25. Catalytic impact of surface modification with BO_x, PO_x, MnO_x: Overview of changing selectivities of desired products and CO_x due to tuned surfaces in (a) ethane-, (b) propane-, and (c) *n*-butane oxidation for the six studied catalysts $MoVTeNbO_x$. $MoVO_x$, MoO_3, V_2O_5, VPP and $SmMnO_3$. The data set represents the absolute change in selectivities and conversion comparing the surface modified sample with the respective base catalyst at a fixed temperature (depending on the catalyst and the reaction, see **Figure SI5** and **Figure SI6**) and fixed conversion of X_{alkane} = 15% (exception: MoO_3 and $SmMnO_3$ is shown at X_{alkane} = 10%); the data set originates from GHSV-variation studies, in which the temperature is fixed for all samples to achieve a broad conversion range by varying the contact time in a range of 500 to 5000 h^{-1}. The complete GHSV variation study can be found in the data set, provided in the SI. $C_2H_6/O_2/H_2O$=3/9/0 %vol, $C_3H_8/O_2/H_2O$=3/9/20 %vol, $C_4H_{10}/O_2/H_2O$=2/20/3 %vol, 1 atm.

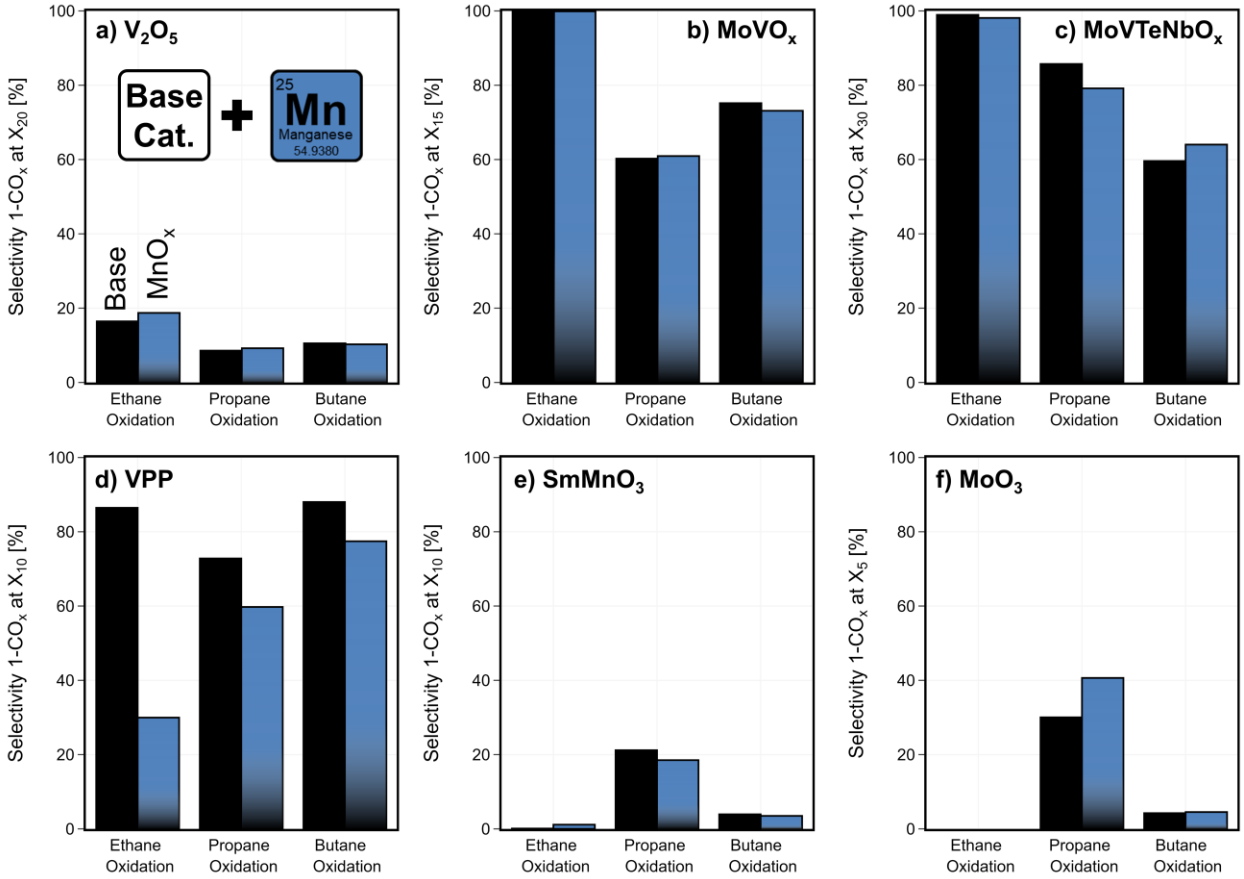

Figure SI26. Change in product formation by the deposition of MnO_x on the surface of the six studied catalysts (a) V_2O_5, (b) $MoVO_x$, (c) $MoVTeNbO_x$, (d) VPP, (e) $SmMnO_3$, (f) MoO_3: Selectivity towards the sum of partial oxidation products (1-CO_x) shown in ethane, propane, *n*-butane oxidation at fixed temperature setpoint for each reaction and catalyst (see contact time variation study Figure SI5 and Figure SI6); the product selectivity is shown at a fixed interpolated alkane conversion level by varying the contact time in a range of 500-5000 h^{-1}; the complete contact time variation study can be found in the data set provided in the SI. $C_2H_6/O_2/H_2O$ = 3/9/0 %vol, $C_3H_8/O_2/H_2O$ = 3/9/20 %vol, $C_4H_{10}/O_2/H_2O$ = 2/20/3 %vol, 1 atm.

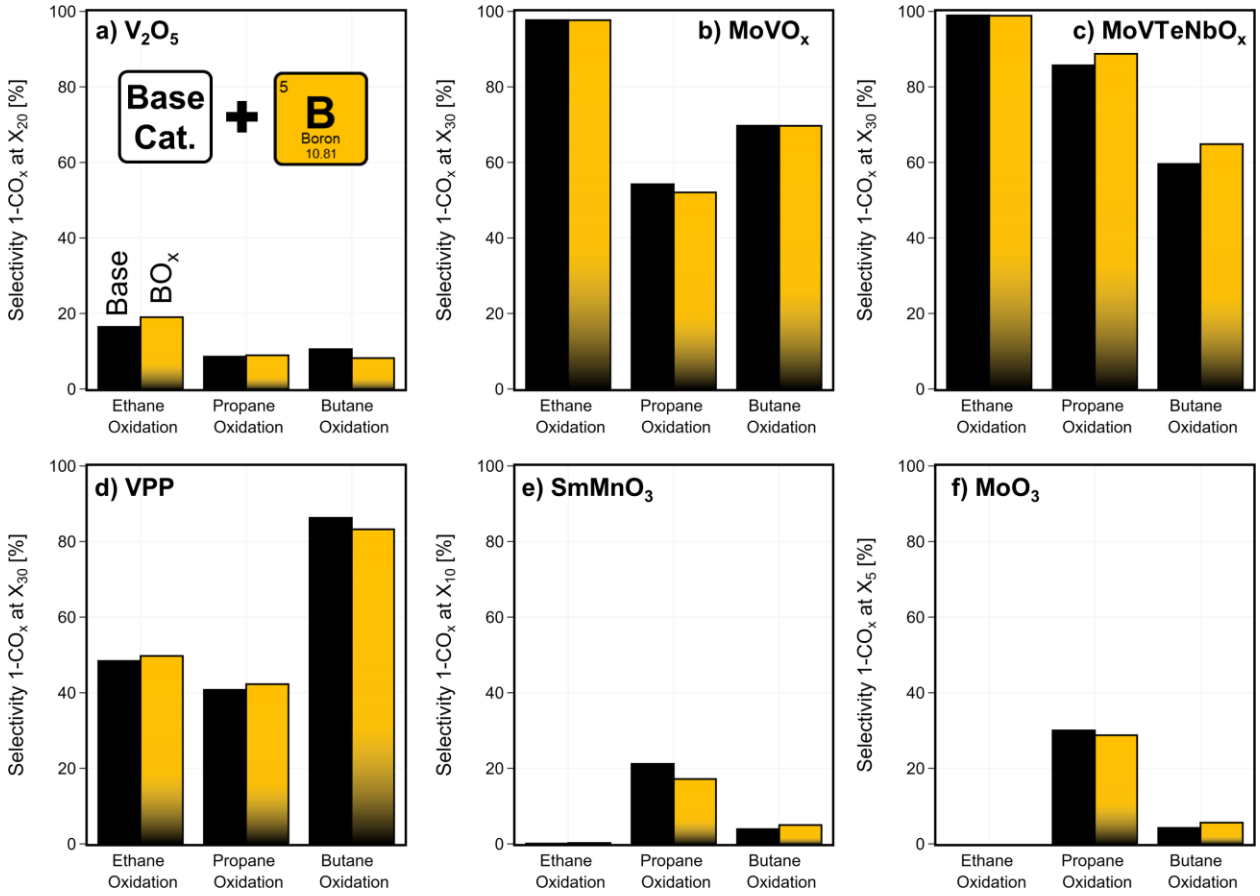

Figure SI27. Change in product formation by the deposition of BO_x on the surface of the six studied catalysts (a) V_2O_5, (b) $MoVO_x$, (c) $MoVTeNbO_x$, (d) VPP, (e) $SmMnO_3$, (f) MoO_3: Selectivity towards the sum of partial oxidation products (1-CO_x) shown in ethane, propane, *n*-butane oxidation at fixed temperature setpoint for each reaction and catalyst (see contact time variation study Figure SI5 and Figure SI6); the product selectivity is shown at a fixed alkane conversion level by varying the contact time in a range of 500-5000 h^{-1}; the complete contact time variation study can be found in the data set provided in the SI. $C_2H_6/O_2/H_2O$ = 3/9/0 %vol, $C_3H_8/O_2/H_2O$ = 3/9/20 %vol, $C_4H_{10}/O_2/H_2O$ = 2/20/3 %vol, 1 atm.

Base catalyst synthesis

$MoVTeNbO_x$. Synthesis adapted from Kolen'ko Y. et al. (2011) [8].

$MoVO_x$. Synthesis according to Trunschke et al. (2017) [9].

MoO_3. Synthesis according to Cotter T.et al. (2013) [10].

V_2O_5. Divanadium pentoxide (V_2O_5, purity 99.6 %, Dallan Galaxy Metal Material Co. Ltd., CAS-Nr. 1314-62-1).

VPP. Vanadyl(IV) pyrophosphate (VPP, $(VO)_2P_2O_7$) was synthesized according to patent literature following an organic route [11].

$SmMnO_3$. Synthesis according to Koch et al. (2020) [12].

References

1 Gallagher, McCarthy. "Penn State University." *University Park, PA, USA, ICDD Grant-in-Aid* **1973**.

2 E. Bordes, P. Courtine, *J Catal* **1979**, *57* (2), 236–252.

3 R. Enjalbert, & J. E. A. N. Galy, *Acta Crystallographica Section C: Crystal Structure Communications*, **1986**, *42*(11), 1467-1469.

4 H. E. Swanson, R. K. Fuyat, G. M. Ugrinic, Natl. Bur. Stand. (U.S.), Circ. 539, III, **1954**, 30.

5 L. Foppa, F. Rüther, M. Geske, G. Koch, F. Girgsdies, P. Kube, S. Carey, M. Hävecker, O. Timpe, A. Tarasov, M. Scheffler, F. Rosowski, R. Schlögl, and A. Trunschke, *J. Am. Chem. Soc.* **2023**, 145 (6), 3427-3442.

6 D. Melzer, P. Xu, D. Hartmann, Y. Zhu, N. D. Browning, M. Sanchez-Sanchez, J. A. Lercher, *Angew. Chem. Int. Ed.* **2016**, 55, 8873.

7 P. DeSanto Jr., D. J. Buttrey, R. K. Grasselli, C. G. Lugmair, A., F. Volpe Jr., B. H. Toby, T.Vogt. *Z. Kristallogr.* **2004**, 219, 152.

8 Y.V. Kolen'ko, W. Zhang, R. Naumann d'Alnoncourt, F. Girgsdies, T.W. Hansen, T. Wolfram, R. Schlögl, and A. Trunschke, *ChemCatChem*, **2011**, 3: 1597-1606.

9 A. Trunschke, J. Noack, S. Trojanov, F. Girgsdies, T. Lunkenbein, V. Pfeifer, M. Hävecker, P. Kube, C. Sprung, F. Rosowski and R. Schlögl, *ACS Catalysis*, **2017**, 7, 3061–3071.

10 T. Cotter, B. Frank, W. Zhang, R. Schlögl, and A. Trunschke, *Chemistry of Materials*, **2013** 25 (15), 3124-3136.

11 J. Weiguny, S. Storck, M. Duda, C. Dobner, European Patent 1487576(A1), **2003**.

12 G. Koch, M. Hävecker, D. Teschner, S. J. Carey, Y. Wang, P. Kube, W. Hetaba, T. Lunkenbein, G. Auffermann, O. Timpe, F. Rosowski, R. Schlögl and A. Trunschke, *ACS Catalysis*, **2020**, 10, 7007–7020.